2016

Biomechanics of Retinal Venous Pulsations as Indicators of Intracranial Pressure

Charles F. Babbs
Purdue University, babbs@purdue.edu

Biomechanics of Retinal Venous Pulsations as Indicators of Intracranial Pressure

Charles F. Babbs, MD, PhD

Weldon School of Biomedical Engineering, Purdue University,
West Lafayette, Indiana, United States of America.
E-mail: babbs@purdue.edu

Abstract

The origin of retinal venous pulsations remains an open problem in physiology and medicine; so too, their exact relationship to intracranial pressure. This study takes a mathematical modeling approach to explore details of blood flow through the eye to reveal the mechanism of pulsations. The intravaginal, intraneural, and intraocular segments of the retinal arteries and veins are modeled as connected resistive-capacitive segments. The analysis incorporates two critical mechanical properties of these small blood vessels, not heretofore studied, which become significant under conditions of negative transmural pressures: (1) dramatically reduced compliance during flattening and (2) cross-sectional shape change as internal volume decreases. Intraocular pressure acting on these veins close to the optic disc normally creates fluctuating negative transmural pressure. The observed long diameters of these venous segments become wider during diastole as they empty and flatten and narrower during systole as they refill with blood. Such visible pulsations occur only in models that include nonlinear compliance and constant-perimeter flattening. Further, the pulsations disappear when raised intracranial pressure, raised cavernous sinus pressure, or reduced arteriolar resistance elevates internal pressure in all retinal veins above the level of intraocular pressure. In this case transmural venous pressures are always positive, cross sectional shapes are circular, and compliance is greatly reduced. Then visible retinal venous pulsations disappear. Scenarios are suggested under which intracranial pressure can be estimated quantitatively from physical examination of retinal venous pulsations, if intraocular pressure is also measured.

Key words: cerebrospinal fluid pressure, intracranial hypertension, intracranial pressure, spontaneous venous pulsations

Introduction

Retinal veins are often seen to pulsate on direct ophthalmoscopic examination of the eye, whereas most systemic veins do not obviously pulsate. The spontaneous retinal venous pulsations appear as time-varying changes in the observed diameters of larger retinal veins as they cross the optic disc. The veins pulsate in rhythm with the cardiac cycle, contracting during systole and expanding during diastole[1-3]. These spontaneous venous pulsations are present in about 83% of normal persons[4]. Typically the change in retinal vein diameter observed in the sitting or upright position is in the range of 5 to 30 percent. In some cases there can be as much as 66% change in the observed vessel diameter[4].

Retinal venous pulsations have some curious features. They are most prominent in larger retinal veins near the optic disc, especially in the final segments crossing the disc, even though intravascular pressures are lower in these segments than in upstream retinal veins. The apparent expansion of retinal veins does not correspond to peak pressure or peak flow. Instead, expansion of the downstream retinal veins occurs in mid to late diastole. The disappearance of retinal venous pulsations is associated with increased intracranial pressure and cerebrospinal fluid pressure. However, return of spontaneous venous pulsations in this situation can be caused by finger pressure on the eyeball (globe) which increases external pressure on the retinal veins[5].

Spontaneous venous pulsations have potential utility as non-invasive indicators of intracranial pressure or cerebrospinal fluid pressure. They are reported to disappear with a cerebrospinal fluid pressure above 20 cmH_2O (15 mmHg)[5-8]. Interestingly, in patients in whom spontaneous venous pulsations do not appear to be present, the pulsations often can be induced by digital pressure on the globe through the eyelid[5]. In some cases pulsations can be elicited or accentuated by the increased intraocular pressure in glaucoma[1]. Further, the phenomenon may be influenced by sitting vs. recumbent positions[4], which change both intracranial pressure and downstream venous pressure in the cavernous sinus.

Raised intracranial pressure is important to detect clinically, both because it can indicate an expanding mass lesion, such as a brain tumor or hematoma, and because raised intracranial pressure by itself can compromise capillary blood flow in the brain by compressing capillaries and small veins and increasing cerebrovascular resistance. A well known clinical rule of thumb states that the presence of spontaneous venous pulsation excludes raised intracranial pressure[9,10], so that cessation of spontaneous venous pulsations is an important clinical sign of raised intracranial pressure, especially in monitoring patients who are likely to develop intracranial hypertension for reasons such as brain tumor or head trauma. Classically, Levin[1] found that spontaneous venous pulsations were present in 88% of 146 unselected adult humans in the sitting position and absent in 100% of patients with raised intracranial pressure above 19 cmH_2O. However, because the absence of pulsations may be found with normal intracranial pressure, neither the presence nor absence of spontaneous venous pulsations is sufficient to conclude that the intracranial pressure is normal[5]. Wong and White[4] found that of 26 patients with raised intracranial pressure (> 22 cmH_2O) only 10 had absent spontaneous venous pulsation. In the combined population of patients with either normal or raised intracranial

pressure, the proportion of patients with absent spontaneous venous pulsations who had high intracranial pressure was 17 percent. Thus, although potentially useful as indicators of intracranial pressure, retinal venous pulsations provide a somewhat uncertain guide for clinical decision making, especially because the exact cause of the pulsations and the factors contributing to their appearance and disappearance are not known.

The present study uses a biomechanical and mathematical modeling approach to create a new theory of retinal venous pulsations that incorporates two physical characteristics of retinal veins not heretofore considered: non-linear compliance and bending deformation. Thin walled elastic tubes such as veins exhibit nonlinear compliance when they transition between expanding and flattening deformation, as transmural pressure varies from positive to negative. Deformation by "ovalization" and flattening of the veins under negative transmural pressure causes their observed long diameters to increase in size, even as internal blood volume decreases. The proposed new theory generates quantitative predictions of the amplitude of retinal venous pulsations under a wide variety of physiological scenarios with varying intraocular pressures, intracranial pressures, central venous pressures, and retinal artery diameters, including the conditions under which they appear and disappear, providing new insights into their value as indicators of raised intracranial pressure.

Glossary

C	Segmental vascular compliance (ml/(dyne/cm^2))
d	Internal diameter of a vascular segment (cm)
$\hat{d}_0$	Internal diameter of a vascular segment under zero transmural pressure (cm)
E_{wall}	Young's modulus of elasticity of a vascular segment wall (dynes/(cm^2))
ε	Fraction of total resistance to blood flow attributable to capillary beds
h	Wall thickness of a vascular segment (cm)
i_k	Instantaneous blood flow between segments k and k+1 (ml/sec)
L	Length of a vascular segment (cm)
MAP	Mean arterial pressure (mmHg)
μ	Blood viscosity (dyne-sec/cm^2)
ω	Angular frequency of the heartbeat (Hz)
P_a	Ophthalmic artery pressure (mmHg)
P_v	Cavernous sinus pressure (mmHg)
PP	Arterial pulse pressure (mmHg)
R_{cap1}	Resistances of distal capillary beds to blood flow (mmHg/(ml/sec))
R_{cap2}	Resistance of proximal capillary beds to blood flow (mmHg/(ml/sec))
r	Internal radius of a vascular segment (cm)
R	Segmental vascular resistance (mmHg/(ml/sec))
$\hat{R}_0$	Resistance of a vascular segment under zero transmural pressure (mmHg/(ml/sec))
Δt	Time step for numerical integration (sec)
V	Volume of a vascular segment (ml)
$\hat{V}_0$	Unstressed volume of a vascular segment with zero transmural pressure (ml)
ΔV	Change in segmental volume during time step Δt (ml)

Model development

Underlying anatomy for the model

A successful mathematical and computational model of retinal venous pulsations must be faithful to some relatively arcane and subtle features of ocular anatomy, including the courses of retinal arteries and veins through the subarachnoid space, optic nerve stem, and the globe of the eye. Along this complex pathway, the walls of retinal arteries and veins are subjected, not only to internal blood pressure, but also to external pressure provided by the cerebrospinal fluid in the intravaginal space (the sleeve of dura-covered subarachnoid space surrounding the optic nerve), to any pressure transmitted through the substance of the optic nerve, and to intraocular pressure within the globe.

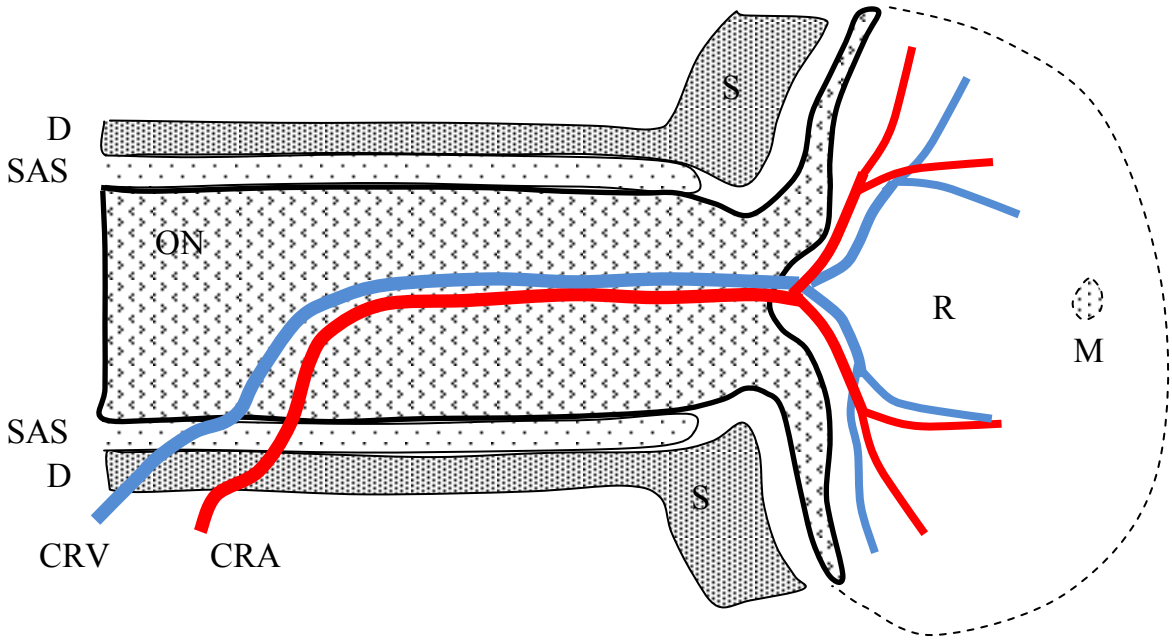

Fig 1. Schematic representation of the course of the central retinal artery and vein, near and within the optic nerve. CRA = central retinal artery; CRV = central retinal vein; D = dura; M = macula; ON = optic nerve; R = retina; S = sclera; SAS = subarachnoid space. Sketched from Hayreh[11] and Anand-Apte (http://fliphtml5.com/cqtz/noua).

The course of the central retinal artery is complex and can have many anatomic variations[11]. Fig 1 illustrates a typical case, based on the study of Hayreh[11]. The central retinal artery is a

branch of the ophthalmic artery, which itself branches from the internal carotid artery. To reach the optic nerve stem it traverses a layer of dura mater and a short segment of the subarachnoid space, dives into the substance of the optic nerve to a position near the central axis of the nerve, and then traverses the central axis of the optic nerve for a distance of about 10 mm, where it passes into the globe and branches typically into 4 quandrantal arteries (the superior and inferior nasal and temporal arteries) to supply the surface of the retina. Tiny retinal venules collect capillary blood in a fishbone-like pattern and drain into companion quadrantal veins, which join over or near the optic nerve head to form the central retinal vein (Fig 2). These retinal veins are subjected to intraocular pressure. The central retinal vein then dives into the substance of the optic nerve near the center of the optic cup and traverses the core of the optic nerve stem, usually close to the central retinal artery, where it is largely protected from flattening caused by cerebrospinal fluid pressure in the subarachnoid space (Appendix 1 and also Fry[12]). Then the central retinal vein turns sharply and proceeds toward the periphery of the nerve to emerge and run along the side of the nerve through the intervaginal space for about two to three millimeters[11], where it is subjected directly to cerebrospinal fluid pressure, rendering it particularly vulnerable to compression by raised fluid pressure in this space[12], before it penetrates the dura to connect with the superior ophthalmic vein, which in turn drains into the cavernous sinus and ultimately, via the petrosal sinus, into the jugular vein.

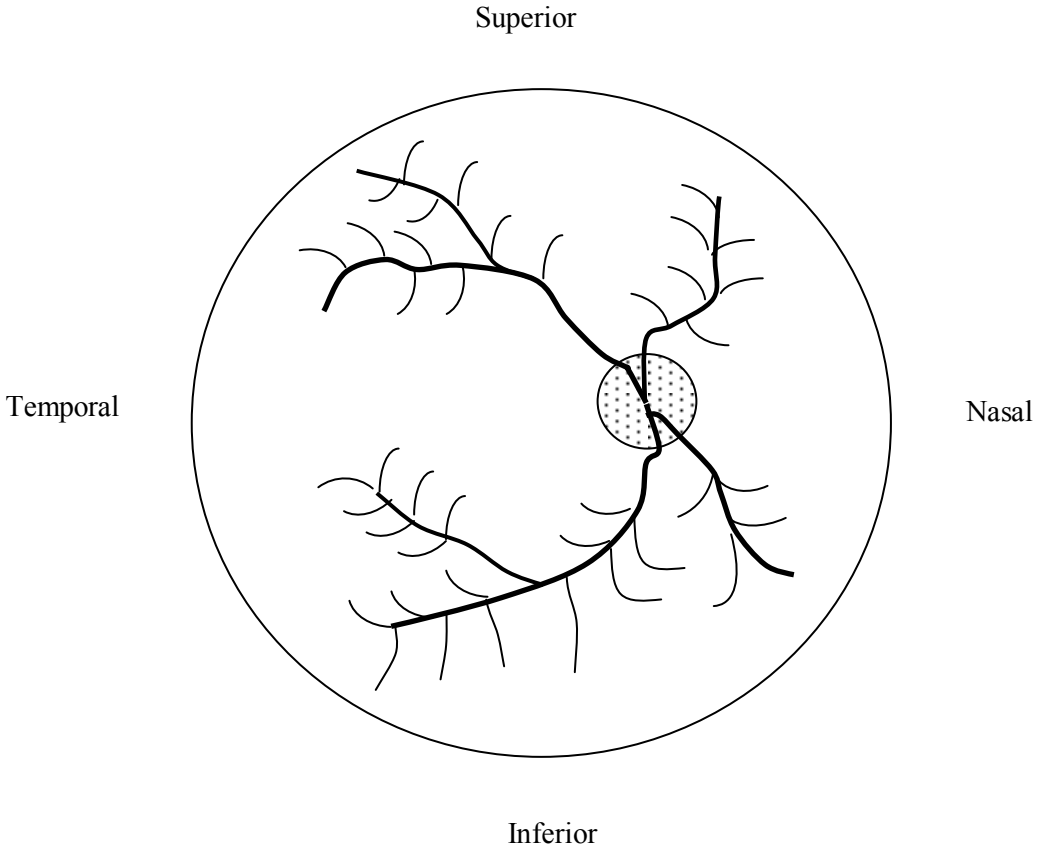

Fig 2. Layout of branches of the four principal retinal vessels of the right eye with fishbone or herringbone-like pattern of venules draining into quadrantal retinal veins.

Several other features that are important for inclusion in a hemodynamic model include the relatively non-compliant sclera of the globe that allows for build up of intraocular pressure, the internal dimensions and wall thicknesses of the retinal vessels, the thickness and stiffness of the optic nerve stem, the calibers and lengths of the various vascular segments, and the action of intraocular pressure that is transmitted to intraocular vessels by the gel-like vitreous body, compressing them against the retina and underlying sclera with a bias toward ovalization and flattening.

Layout of the model

Fig 3 shows the mathematical and computational model analogous to the forgoing anatomical and physiological system. The model consists of 8 compartments representing segments of blood vessels. Each vascular segment has a characteristic compliance and a characteristic resistance. In this mathematical analog the segmental compliance is flanked by half of the segmental resistance on each side to create an RC network component. These components are connected in series to represent the vascular path through which blood flows from the ophthalmic artery, through the globe, to the ophthalmic vein.

Subscripts 1 through 8 represent vascular components in the model. Variables R and C represent local segmental resistances and compliances. R_1 and C_1 represent the central retinal artery segment traversing the subarachnoid space between the dura and the optic nerve. The input internal arterial pressure for segment 1 is equal to the time-varying ophthalmic artery pressure, denoted P_a. R_2 and C_2 represent the intraneural portion of the central retinal artery. R_3 and C_3 represent the four lumped quadrantal retinal arteries within the globe--the superior and inferior temporal retinal arteries and the superior and inferior nasal retinal arteries. Because the focus of the model is on retinal veins and venous pulsations, extra compartments are used to represent the more peripheral, more central, and most central venous segments. The most central venous segments are located over or near the optic disc and commonly exhibit spontaneous venous pulsations. R_4 and C_4 represent the more peripheral retinal veins relatively far from the optic disc. R_5 and C_5 represent the more central retinal veins closer to the optic disc. R_6 and C_6 represent the most central retinal veins within two disc diameters of the center of the optic disc. R_{cap1} and R_{cap2} represent the many lumped capillaries and venules that drain into venous compartments 4 and 5. R_{cap1} represents capillaries draining into more peripheral retinal veins, and R_{cap2} represents capillaries draining into more central retinal veins. These smallest vascular channels are regarded as purely resistive. R_7 and C_7 represent the intraneural segment of the central retinal vein. R_8 and C_8 represent the extraneural segment of the central retinal vein within the subarachnoid space, between its point of exit from the optic nerve to its point of penetration through the dura. Compartment 8 of the central retinal vein is subjected to intracranial or cerebrospinal fluid pressure. After exiting the dura, the central retinal vein has internal pressure equal to local ophthalmic venous pressure, P_v, which is considered a constant in time.

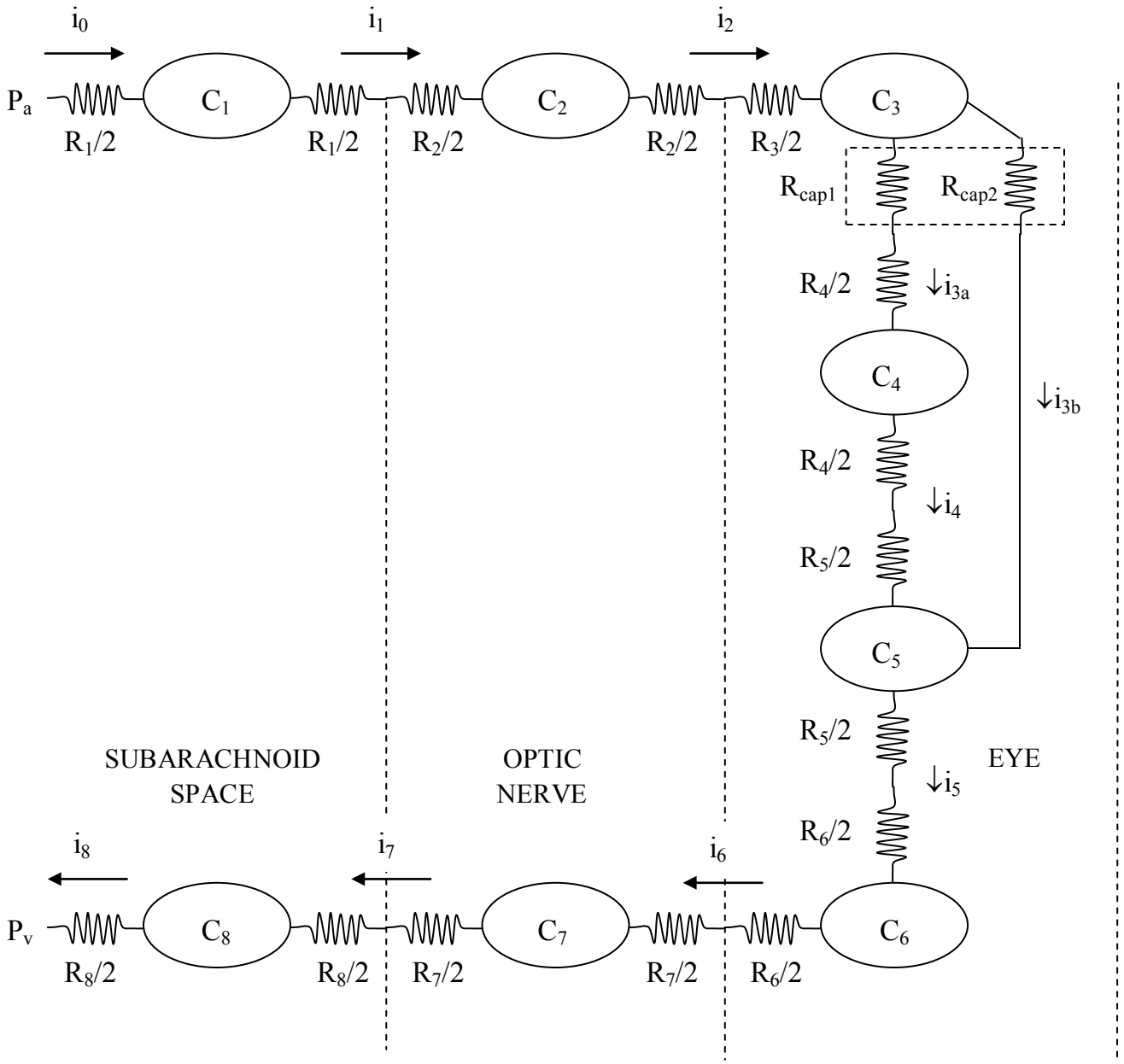

Fig 3. Model of blood flow through the eye. C_1 and C_2, compliances of segments of central retinal artery; C_3, compliance of 4 parallel retinal arteries (4x that of one retinal artery); C_4, compliance of 4 parallel segments of distal retinal veins; C_5, compliance of 4 parallel segments of more downstream retinal veins; C_6, compliance of 4 parallel segments of the most downstream central retinal veins; C_7, compliance of the intraneural segment of the central retinal vein; C_8, compliance of the intravaginal segment of the central retinal vein within the subarachnoid space. R_1 and R_2, intravaginal and intraneural segments of the central retinal artery, R_3, parallel intraocular retinal arteries having ¼ the resistance of individual retinal artery segments; R_{cap1} and R_{cap2}, resistances of more distal and more central capillary beds in parallel; R_4, R_5, R_6, ¼ the resistance of individual retinal vein segments; R_7 and R_8, intraneural and intravaginal retinal venous segments; P_a, arterial pressure; P_v, cavernous sinus pressure.

Compliances

The compliances of arterial and venous segments are computed using the classical formula for thin walled elastic tubes[13]

$$C = \frac{2\pi L r_i^3}{E_{wall} h}, \qquad (1)$$

where L is the length of the tube, r_i is the internal radius, and h is the wall thickness. Values of these variables are provided in Table 1. E_{wall} is Young's modulus of elasticity of the blood vessel wall (proportional to stiffness). A mid-range value for Young's modulus of blood vessel wall material is taken as 5×10^6 dynes/cm^2 after Bergel[14]. To represent greatly increased compliance during bending and flattening, the compliance given by Equation (1) for cylindrical expansion of any vascular segment is multiplied by a factor of 20, based on the data of Moreno and coworkers[15], whenever segmental volume is less than the unstressed volume, that is $V < \hat{V}_0$.

Table 1. Model parameters.

Model segment	Length (cm)	Radius (cm)	n parallel	Thickness[1] (cm)	Compliance[1,2] (cm^5/dyne)	Volume (cm^3)	R (dyne-sec/cm^5)
1	0.30	0.015	1	0.0030	4.24E-10	2.12E-04	4.53E+05
2	1.20	0.015	1	0.0030	1.70E-09	8.48E-04	1.81E+06
3	1.50	0.005	4	0.0010	9.42E-10	4.71E-04	4.59E+07
4	0.70	0.006	4	0.0010	7.60E-10	3.17E-04	1.03E+07
5	0.70	0.006	4	0.0010	7.60E-10	3.17E-04	1.03E+07
6	0.10	0.006	4	0.0010	1.09E-10	4.52E-05	1.47E+06
7	1.20	0.015	1	0.0015	3.39E-09	8.48E-04	1.81E+06
8	0.30	0.015	1	0.0015	8.48E-10	2.12E-04	4.53E+05
Cap							1.81E+07

Notes:

1. Central retinal artery and vein diameters and wall thicknesses from Gray's Anatomy: upload.wikimedia.org/wikipedia/commons/3/3a/Gray880.png, combined with data from Lagreze et al.[16], from Pathology Education Informational Resource (PEIR) Digital Library -- peir.path.uab.edu/library/picture.php?/29521, based upon optic nerve diameters from Lagreze et al.[16]. Intraocular retinal artery and vein diameters from Lee et al.[17]

2. Length of intravaginal segments 1 and 8 is taken from the rendering of Fig 1, assuming the distance from the point of penetration of the dura by the central retinal artery and the globe is approximately 12 mm in an average person.

Volumes

The initial volumes of vascular compartments at time zero of the simulation are specified by the lengths and radii given in Table 1 and are denoted V_{normal}. Volumes V_{normal} correspond to typical normal internal pressures, P_{normal}, for example 90 mmHg for arterioles and 20 mmHg for venules. The unstressed volumes (zero transmural pressure) are denoted $\hat{V}_0$ and are given by

$$\hat{V}_0 = V_{normal} - C(P_{normal} - P_{ext}), \tag{2}$$

where C is the local segmental compliance in expansion, and P_{ext} is the local external pressure, which may be cerebrospinal fluid pressure or intraocular pressure.

Changes in segmental vascular volumes during time increment, Δt, depend on blood flow entering the segment, i_{in}, and blood flow exiting the segment, i_{out}, and are specified as

$$\Delta V = (i_{in} - i_{out})\Delta t \text{ , if } V > -\hat{V}_0 ,$$
$$\Delta V = 0 \text{ , if } V \le -\hat{V}_0 \text{ and } i_{in} < i_{out}. \tag{3}$$

In this way negative volumes, less than $-\hat{V}_0$, are not allowed.

Resistances

The initial resistances of arterial and venous segments having a circular cross-section are computed using Poiseuille's Law

$$R = \frac{8L\mu}{\pi r_i^4}, \text{ when } V \ge \hat{V}_0 , \tag{4}$$

where μ is blood viscosity with a numerical value of 0.03 dyne-sec/cm^2. For retinal veins that become ovalized and flattened at volumes less than their unstressed volumes ($V < \hat{V}_0$) local segmental vascular resistances are estimated by the expression

$$R = \frac{\hat{R}_0}{a^4 + 4a^2(1-a)}, \tag{5}$$

as derived in Appendix 3, where $a = 1 - \sqrt{1 - V/\hat{V}_0}$ and $\hat{R}_0$ is the unstressed segmental resistance from Poiseuille's Law for internal pressure equal to external pressure and $V = \hat{V}_0$.

Total capillary resistance is computed using the textbook relationship[18] from cardiovascular physiology that the pressure drop across capillary beds is a small fraction, ε, approximately 20 percent, of the total pressure drop across the systemic vascular bed from aorta to right atrium. In this case for unknown capillary resistance, R_{cap}, we have

$$\varepsilon = \frac{R_{cap}}{R_{art} + R_{ven} + R_{cap}}, \tag{6}$$

where R_{art} is the total arterial resistance leading to a particular vascular bed and R_{ven} is the total venous resistance draining the vascular bed. In terms of normal series resistances, R_i, in Table 1 with ε = 0.2

$$R_{cap} = \frac{\varepsilon}{1-\varepsilon}\left(R_{art} + R_{ven}\right) \approx \frac{1}{4}\sum_{i=1}^{8} R_i \,. \tag{7}$$

In the model of Fig 3 the capillary resistance is regarded as having two parallel components, the first representing the half of retinal capillary beds that feed the more peripheral veins, and the second representing the half of retinal capillary beds that feed more central retinal veins in the fishbone pattern of Fig 2. In this case, because the two halves are hemodynamically in parallel,

$$R_{cap1} = R_{cap2} = 2R_{cap} \approx \frac{1}{2}\sum_{i=1}^{8} R_i \,. \tag{8}$$

Pressures

Time-varying arterial pressure, P_a, is simulated using a truncated Fourier series[13] of the form

$$P_a(t) \approx MAP + 0.36 \cdot PP \cdot \left[\sin(\omega t) + \frac{1}{2}\sin(2\omega t)\right], \tag{9}$$

where MAP is mean arterial pressure, PP is pulse pressure (systolic minus diastolic) and ω is the angular frequency of the heartbeat (2π times the cardiac frequency in Hz). This function gives a good approximation of a slightly damped aortic pressure waveform expected to be present in the ophthalmic artery. In standard models the numerical values of MAP and PP are 100 mmHg and 40 mmHg. Heart rate is 80 beats/min with angular frequency ω = 8.4 Hz. Venous pressure P_v is taken as a small positive value, 1 mmHg, assuming that the jugular veins in the upright posture act as "vascular waterfalls"[19]. Normal cerebrospinal fluid pressure is taken as 13 mmHg after the data of Avery et al.[20] Normal intraocular pressure is taken as 16 mmHg.

Transmural pressures in vascular segments 1 through 8 are denoted P_1 through P_8. In the circulation to the eye some segments are subjected to external pressures, either as they traverse

the subarachnoid space, where the external pressure equals the intracranial or cerebrospinal fluid pressure, or as they traverse the retina, where the external pressure equals the intraocular pressure. In segments 1 and 8, surrounded by cerebrospinal fluid in the subarachnoid space, the internal pressure in the thin walled elastic blood vessels is augmented by cerebrospinal fluid pressure. In segments 3 through 6 within the globe the internal pressure in the thin walled elastic blood vessels is augmented by intraocular pressure.

In segments 2 and 7, representing the intraneural courses of the central retinal artery and central retinal vein, the internal vascular pressures are shielded from the direct effects of cerebrospinal fluid pressure in the optic nerve subarachnoid space by a relatively thick protective layer of the nerve. This conclusion comes from application of the Lame equations for thick walled pressure vessels to the optic nerve stem (Appendix 1). These calculations show rather convincingly that pressure is not transmitted effectively from the optic nerve subarachnoid space to the intraneural portion of the central retinal vein, the diameter of which would change less than 10 percent with large pathologic increases in cerebrospinal fluid pressure. Surrounded by a relatively thick wall of nerve tissue, the intraneural central retinal vein does not undergo ovalization and flattening like a thin walled elastic tube, when cerebrospinal fluid pressure is greater than local venous pressure, but instead experiences only modest cylindrical contraction. This conclusion is supported also by the observations of Fry[12] who found that there was minimal compression of the intraneural central retinal vein in patients with papilledema, but obvious and dramatic compression of the intravaginal portions of the vein traversing the subarachnoid space, where the biomechanics become those of a thin walled pressure vessel, rather than a thick walled pressure vessel.

Blood flow

Blood flows between compartments, denoted i_0 through i_8 in Fig 3, can be specified in terms of Ohm's Law:

$$
\begin{aligned}
i_0 &= \frac{P_a - P_1}{R_1/2} \\
i_n &= \frac{P_n - P_{n+1}}{(R_n + R_{n+1})/2}, \; n = 1, 2, 4 \text{ through } 7 \\
i_{3a} &= \frac{P_3 - P_4}{R_{cap1} + R_4/2}, \; i_{3b} = \frac{P_3 - P_5}{R_{cap\,2}} \\
i_8 &= \frac{P_8 - P_v}{R_8/2}.
\end{aligned}
\qquad (10)
$$

At the scale of the microcirculation any inertial effects can be ignored, and flow is entirely resistive.

Pulsatile changes in vascular diameters

Changes in vascular diameters depend upon changes in vascular volumes caused by blood flow. For cylindrical deformation in expansion it is clear that

$$\frac{d}{\hat{d}_0} = \sqrt{\frac{V}{\hat{V}_0}} \text{ , when } V \geq \hat{V}_0 . \qquad (11)$$

However, when $V < \hat{V}_0$ thin walled elastic tubes undergo ovalization and flattening[15,21-24]. One diameter elongates and the orthogonal diameter shortens. The perimeter remains essentially constant, owing to bending deformation without stretching or compression in the hoop dimension. In observation of retinal blood vessels using the direct ophthalmoscope the long diameter is seen as vessels are compressed between the gel-like vitreous body and the retina, supported by the much stiffer underlying sclera. An exact closed form solution for the relationship between $d/\hat{d}_0$ and $V/\hat{V}_0$ in this regime is not possible; however a reasonable approximation, as derived in Appendix 2, is

$$\frac{d}{d_0} = 1 + 0.57\sqrt{1 - \frac{V}{\hat{V}_0}} \text{ , when } V < \hat{V}_0 . \qquad (12)$$

This approximation works well for mild to moderate degrees of flattening, as observed in retinal veins[4].

Numerical methods

The forgoing model was implemented numerically using Microsoft Visual Basic code. Critical initial conditions are described in Table 1. At time zero the arterial pressure is that defined by Equation (9) and other pressures are set to approximate normal values. Unstressed volumes are computed for reference using Equation (2). As time progresses, pressures and flows reach stable periodic values over successive cardiac cycles.

Numerical integration is done by computing and updating the following variables, in order, at each successive time step, $\Delta t = 0.01$ millisecond: arterial pressure, P_a; local vascular resistances, R; local flows, i; volume increments, dV; updated volumes, V; pressure increments dP, including nonlinear compliance characteristics for $V < \hat{V}_0$; updated pressures, P, including external intraocular pressure or intracranial pressure; and updated long diameter ratios, $d/\hat{d}_0$. The looping algorithm creates a marching solution for key model variables as a function of time. After one cardiac cycle stable periodic functions are generated, indicating steady-state conditions.

Results

Mechanisms of venous pulsations

Fig 4 shows pressures, flows, volumes, and diameters of vascular segments in the standard normal model after reaching steady-state. The pressure, flow, and volume are all in phase with the arterial pulse. There is a gradient of pressure from upstream to downstream segments. In the normal case pressure in venous segment, P_6, representing retinal veins close to the optic disc, is near intraocular pressure. Instantaneous blood flow rates have similar waveforms in phase with the arterial pulse. Flow i_4 is one half that of other flows, owing to the parallel path configuration. Most segments show minimal variation in diameter. However, segment 6 has long diameter ratios greater than 1 but volume ratios less than 1, indicating partial flattening. Relatively large volume and diameter pulsations are seen for this segment. The waveform shape for the long diameter of segment 6 is inverted compared to the pressure or flow waveforms, indicating increased diameter with reduced volume during cardiac diastole.

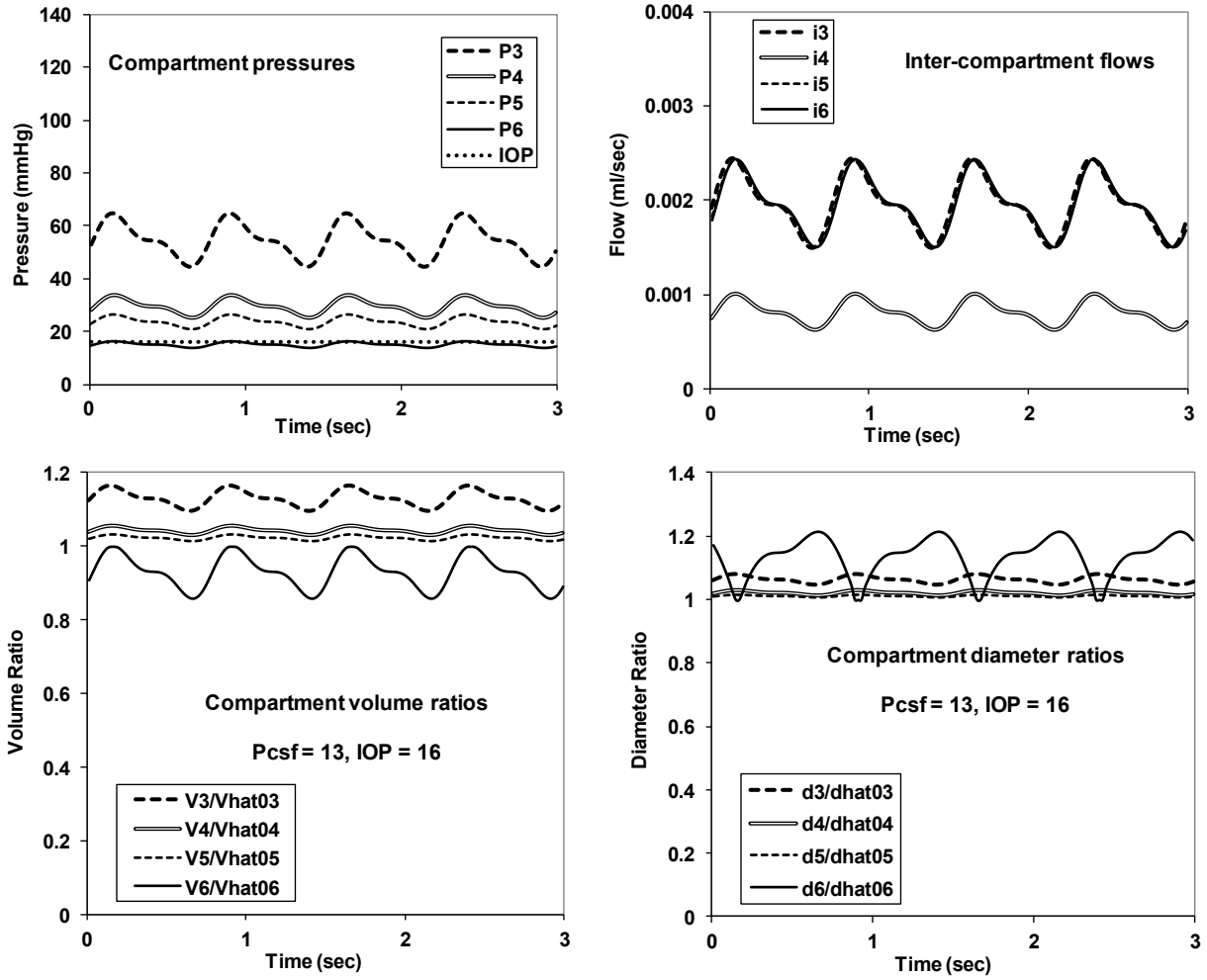

Fig 4. Steady-state time domain records for pressure, flow, volume, and long diameter in the standard model. Time zero represents 0.75 sec after simulation startup. The volume ratio is the ratio of time-varying volume to unstressed volume. The diameter ratio is the ratio of time-varying diameter to unstressed diameter. In the legend, unstressed volumes and diameters are denoted V0 and d0. IOP is intraocular pressure. PCSF is cerebrospinal fluid pressure. P3, V3, and d3 relate to intraocular retinal arteries. Other variables relate to intraocular veins. P6 and V6 correspond to the most downstream retinal veins near the optic disc, which typically show spontaneous pulsations in normal persons. As volume decreases in segment 6, the long diameter increases.

To illustrate the importance of nonlinear compliance during flattening to the generation of retinal venous pulsations, Fig 5 shows time domain plots for otherwise identical simulations in which all vascular compliances remained unchanged at values characteristic of modest positive transmural pressures ($P_i > P_o$). In particular, there is no change in compliance of segment 6 for volumes less than the unstressed volume. In this case the volume in segment 6 is nearly constant and the spontaneous retinal venous pulsations are greatly attenuated.

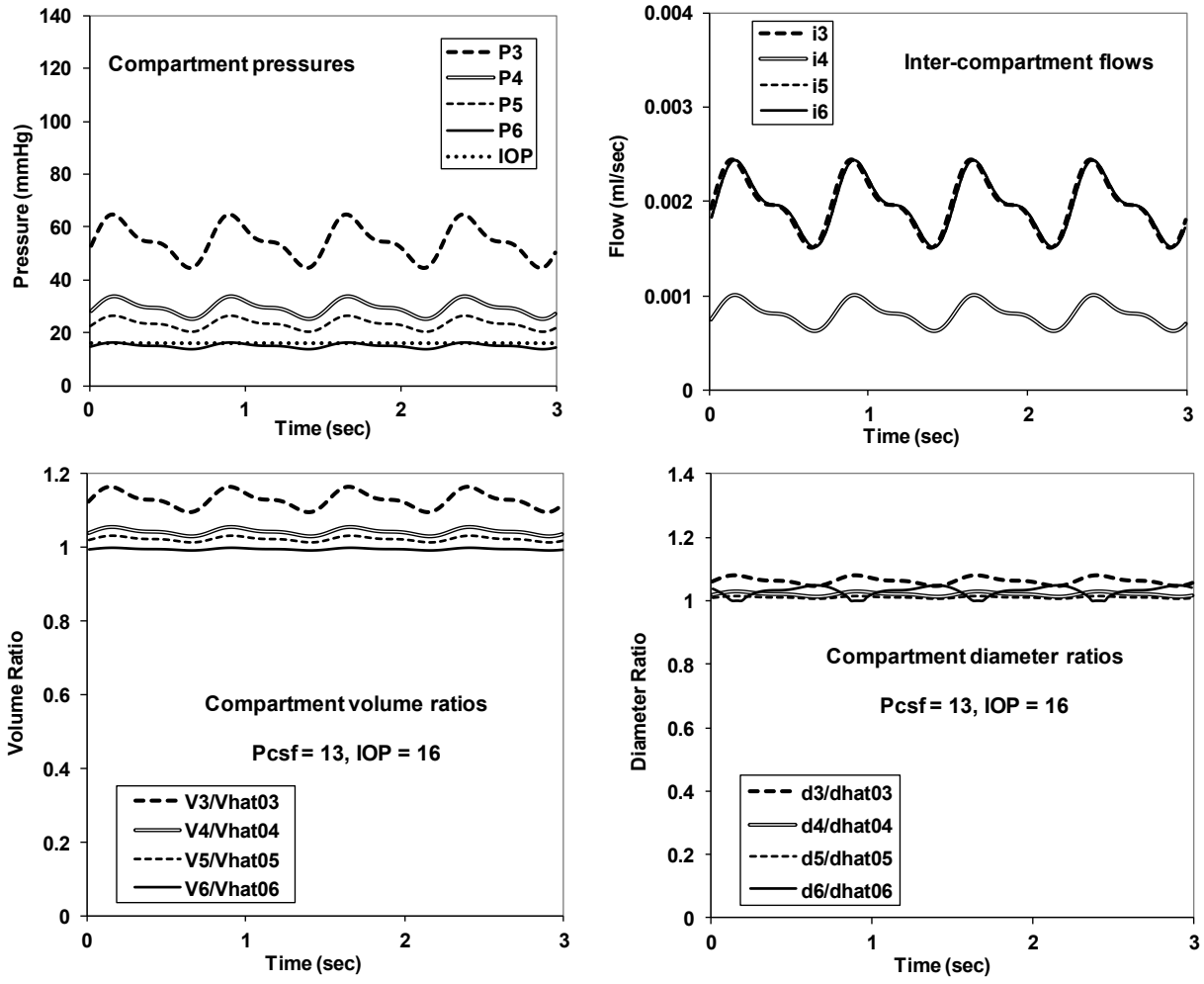

Fig 5. Otherwise standard model with nonlinear compliance turned off in venous compartments 4, 5, 6. Details similar to Fig 4. The inverted diameter pulsations in segment 6 are greatly attenuated.

Varying cerebrospinal fluid pressure

Fig 6(a) shows similar time domain records in an otherwise normal model with P_{csf} increased from 13 to 14 mmHg (18 to 19 cmH_2O). Venous pressure in segment 6 is now greater than intraocular pressure during the first two-thirds of the arterial pulse. The segment is largely operating at positive transmural pressure in the domain of circular expansion. Note the decreased volume and diameter pulses (bottom panels). A further modest increase in cerebrospinal fluid pressure from 14 to 15 mmHg (19 to 20.4 cmH_2O) essentially abolishes the diameter pulsations in segment 6 (Fig 6(b)). There is a sharp threshold for disappearance of the pulses. In Fig 7 pulsatile, peak-to-peak differences in volume and diameter ratios for segment 6 are plotted as a function of cerebrospinal pressure in otherwise standard models. Visible diameter pulsations peak as cerebrospinal fluid pressure approaches intraocular pressure. As cerebrospinal fluid pressure increases above intraocular pressure, there is a sharp drop in visible diameter pulsations.

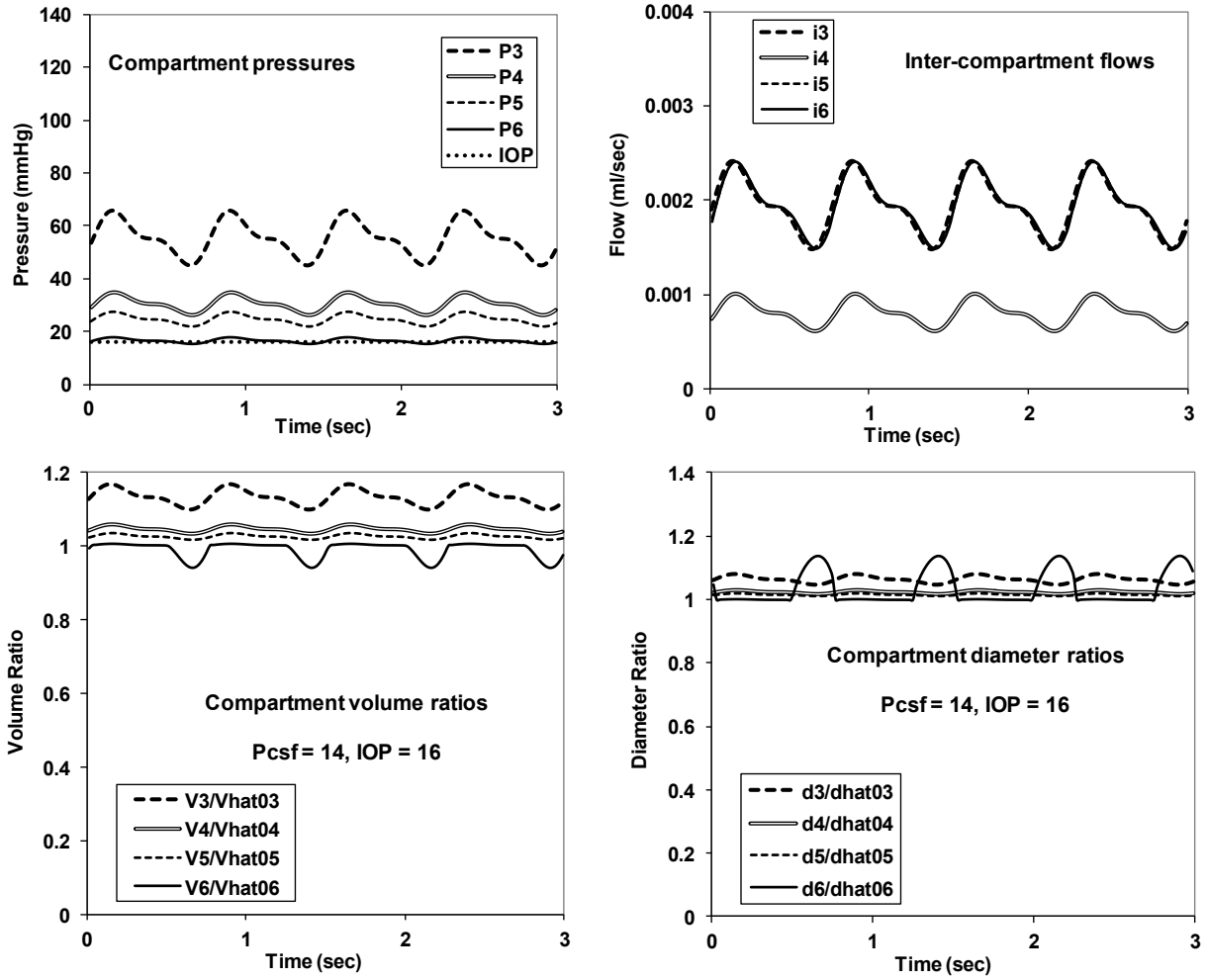

Fig 6(a). Time domain records similar to Fig 5 with P_{csf} increased from 13 to 14 mmHg (18 to 19 cmH_2O).

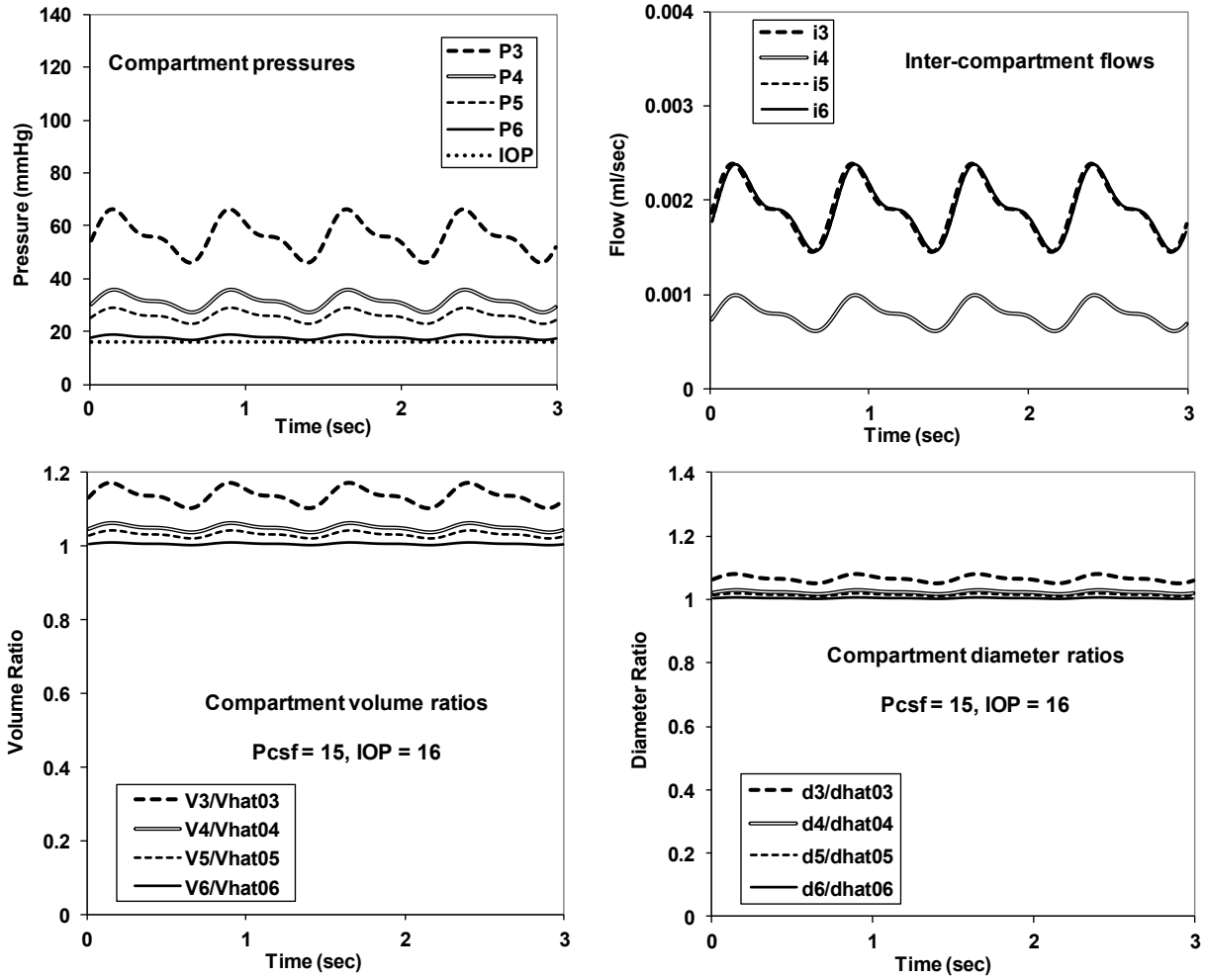

Fig 6(b). Time domain records with P_{csf} increased from 14 to 15 mmHg (19 to 20.4 cmH_2O).

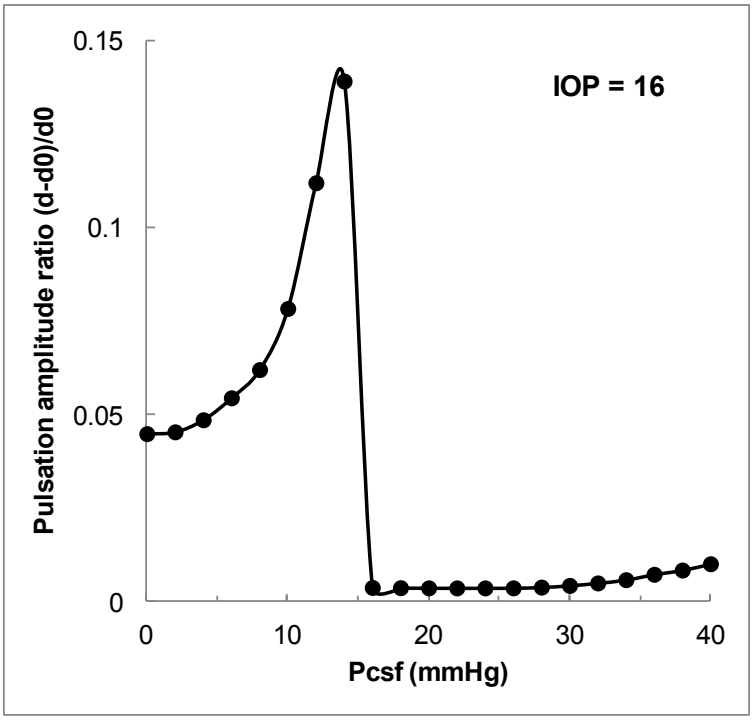

Fig 7. Visible diameter pulsations in retinal vein segments close to the optic disc as a fraction of the unstressed diameter, plotted as a function of cerebrospinal fluid pressure. Pulsation amplitude ratio is the difference between maximal and minimal retinal venous diameter, divided by the unstressed diameter at zero transmural pressure.

The reasons for the dependence of venous pulsations on cerebrospinal fluid pressure are made more clear by examination of the time-domain pressure tracings for segment 6 shown in Fig 8. In the left hand panel, the pressures in segment 6 are less than or equal to intraocular pressure throughout the cardiac cycle (top left). Volumes are consistently less than unstressed volume, as indicated by a volume ratio less than one (middle left). The retinal vein segment is deforming in a highly compliant bending mode, and clear, inverted venous pulsations are seen (bottom left). In the right hand panel pressures in segment 6 are greater than intraocular pressure throughout the cardiac cycle. Volumes are slightly greater than the unstressed volume, as indicated by a volume ratio just slightly greater than one. The retinal vein segment is deforming in a much stiffer stretching mode, and venous pulsations virtually disappear. In the middle panel pressure in segment 6 is sometimes greater and sometimes less than intraocular pressure. Volumes diminish noticeably during bending and "hit the ceiling" of increased stiffness during stretching. Large venous pulsations are seen, associated with the steepest part of the diameter vs. volume curve, which occurs for volumes slightly less than, but close to, $\hat{V}_0$ (See Equation (12) and Fig 13 in Appendix 2.)

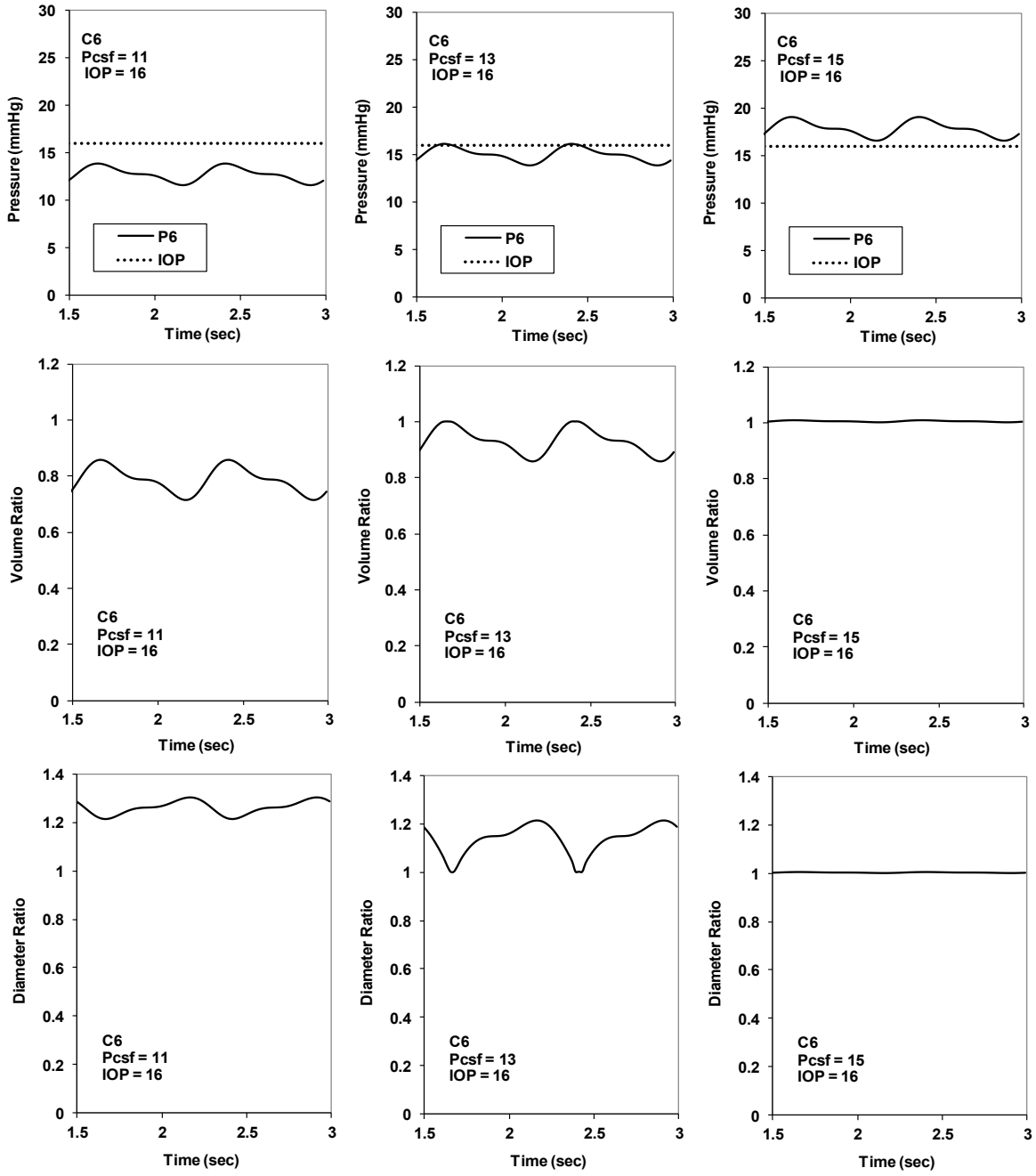

Fig 8. Time domain plots near the threshold for disappearance of retinal venous pulsations. Left panel: intravenous pressure less than intraocular pressure, volume less than 100%, high compliance, bending deformation with ovalization. Right panel: intravenous pressure greater than intraocular pressure, volume slightly greater than 100%, low compliance, stretching deformation with circular expansion. Middle panel: intravenous pressure slightly less than intraocular pressure, volume slightly less than 100%, bending deformation with ovalization in the zone of greatest compliance.

Varying cavernous sinus venous pressure

Fig 9 illustrates the effects upon retinal venous pulsations in segment 6 as outflow venous pressure, P_v, in the ophthalmic vein and cavernous sinus is increased. There is a sharp cutoff corresponding to venous pressures that push internal segment 6 pressures consistently above intraocular pressure. When transmural pressure is consistently positive, pulsations disappear. Considering Fig.s 7, 8, and 9 together, abolition of segment 6 pulsations can be achieved either by raising cerebrospinal fluid pressure or by raising venous pressure in the cavernous sinus.

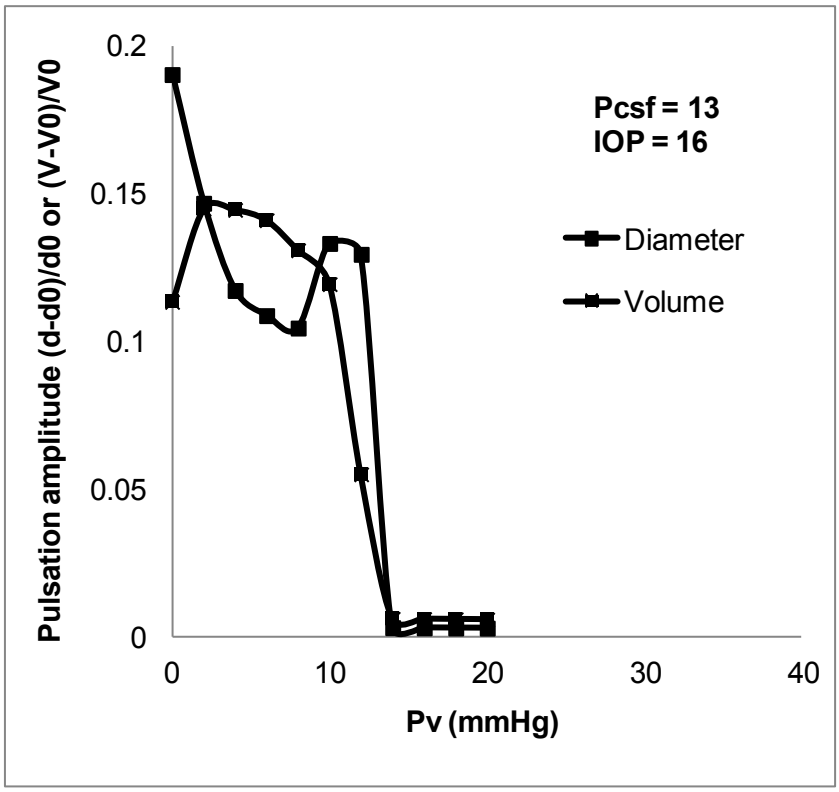

Fig 9. Effects of varying outflow venous pressure on the amplitude of retinal venous pulsations close to the optic disc. Pulsation amplitude ratio is the difference between maximal and minimal retinal venous volume or diameter, divided by the unstressed volume or diameter at zero transmural pressure.

Varying intraocular pressure

A companion phenomenon is shown in Fig 10, where segment 6 pulsation amplitude is plotted as a function of intraocular pressure. In this case there is a sharp appearance of venous pulsations when intraocular pressure rises above the minimal local venous pressure in segment 6.

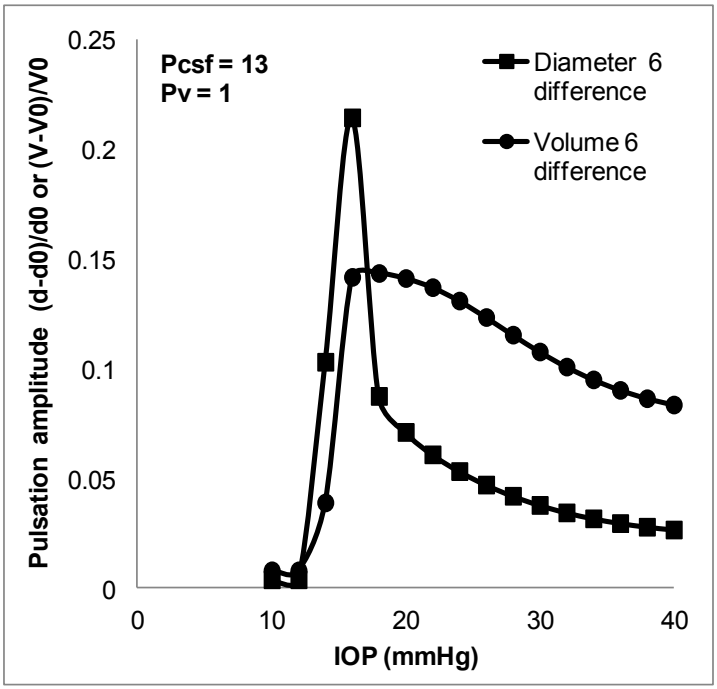

Fig 10. Effect of increasing intraocular pressure on retinal venous pulsations close to the optic disc. Pulsation amplitude ratio is the difference between maximal and minimal retinal venous volume or diameter, divided by the unstressed volume or diameter at zero transmural pressure. These curves are mirror-imaged compared to Figures 7 and 9.

Corresponding time domain plots are shown in Fig 11. With low intraocular pressure (10 mmHg, top, indicated by the dotted line) the local internal pressure in segment 6 is consistently greater than local external pressure, namely intraocular pressure. There is positive distending pressure in the vein. In turn, there is circular stretching deformation, and compliance is relatively low. Pulsations are absent. With intermediate intraocular pressure (15 mmHg, middle) transmural pressure dips into negative territory, where compliance is very high and there is ovalization. At high intraocular pressure (20 mmHg, bottom) transmural pressure is consistently negative. Compliance is high but submaximal. Venous pulsations persist with further ovalization and flattening.

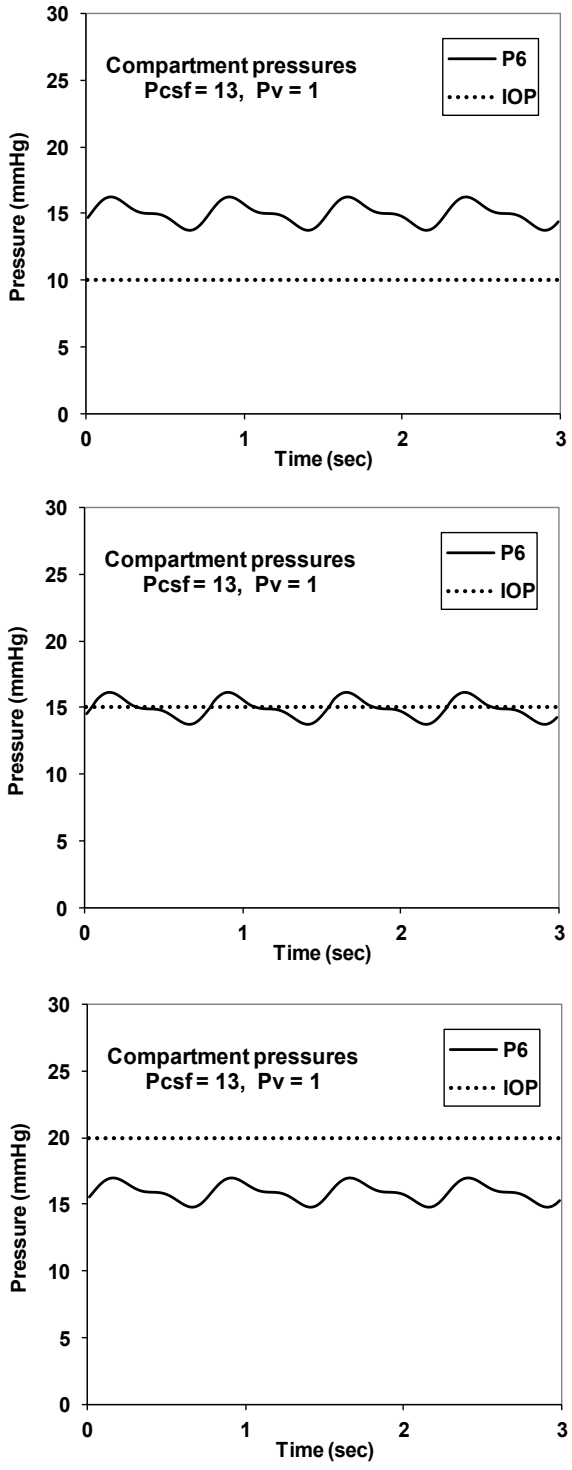

Fig 11. Time domain plots for varying levels of intraocular pressure, indicated here by the dotted line (low, top; high, bottom; intermediate, middle).

Varying arteriolar radius and arteriolar resistance

Fig 12 illustrates the effects of varying internal diameters of intraocular arteries in segment 3 of otherwise standard models. Recall that arteriolar resistance varies inversely as the fourth power of the radius. Hence small changes in radius result in large changes in local vascular resistance. There is a peak of observed venous pulsations close to the optic disc when the arterial radius is near the normal value (50 microns, corresponding to a diameter of 100 microns) as measured by Lee et al.[17] If the arteriolar radius is reduced by half, indicating strong vasoconstriction, the local arteriolar resistance is 16 times greater than normal, and average blood flow is about $1/10^{th}$ normal. There is only trickle flow to downstream veins, where the local venous pressure is about 9 mmHg, compared with intraocular pressure of 16 mmHg. In this case venous volume is about half normal and pulsations are greatly reduced.

On the other hand if the arteriolar radii are increased by a factor of two, indicating strong vasodilation, the local arteriolar resistance becomes $1/16^{th}$ normal. There is robust pulsatile blood flow into the veins. The distending pressure in the most downstream veins close to the optic disc is uniformly positive, between 21 and 26 mmHg, compared with intraocular pressure of 16 mmHg. In this regime of cylindrical expansion venous compliance is low, minimizing observed diameter changes. At the peak amplitude of retinal venous pulsations the arteriolar resistance is large enough so that most of the arterio-venous pressure drop occurs across the arteries. Downstream venous pressure sometimes becomes less than intraocular pressure, and the veins begin to ovalized and flatten. However, the arteriolar resistance remains enough to permit pulsatile blood flow. In this case spontaneous venous pulsations are seen.

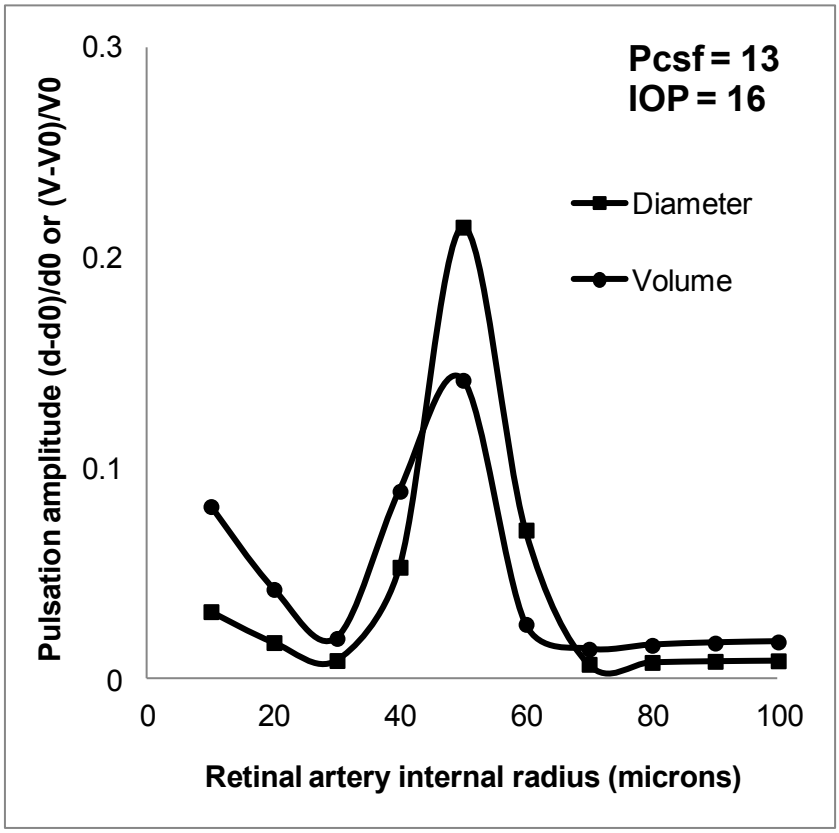

Fig 12. Effects of varying caliber of intraocular retinal arteries on the amplitude of retinal venous pulsations close to the optic disc. Pulsation amplitude ratio is the difference between maximal and minimal retinal venous volume or diameter, divided by the unstressed volume or diameter at zero transmural pressure.

Discussion

The physical principles behind retinal venous pulsations, as well as their proper interpretation as a clinical sign of normal vs. raised intracranial pressure, have been the point of much debate[1,4,5,25]. In particular, the mechanism by which raised intracranial pressure causes loss of spontaneous venous pulsations remains controversial. Levin[1] suggested three possible explanations: (1) increased intraocular blood volume during systole, causing a transient increase of 0.5 to 2.0 mm Hg in intraocular pressure, with a subsequent collapse of veins; (2) a Venturi effect created as blood flows from the multiple peripheral retinal veins into the central retinal vein; and (3) the relatively soft loose connective tissue within the optic disc. Jacks and Miller[5] reviewed proposed mechanisms of spontaneous venous pulsations, including two more possibilities: (4) subtle changes in cerebrospinal fluid pressure (~ 1 mmHg) acting on the central retinal vein as it passes through the subarachnoid space 10 mm behind the globe; and (5) a fluctuating intravascular pressure gradient across the lamina cribrosa between the intraocular and extraocular portions of the central retinal vein. All of these proposed mechanisms are based on semi-quantitative arguments and not on detailed mathematical modeling of the relevant phenomena.

The present study presents a new mechanistic model of retinal venous pulsations and their modification by changes in intracranial pressure. Retinal veins located near the optic disc experience negative transmural pressure under typical normal conditions. During periods of negative transmural pressure these thin walled elastic tubes undergo bending deformation with ovalization, rather than radially symmetrical circular compression. The forces required for bending are much less than those for stretching, with a relatively sharp transition at zero or slightly negative transmural pressure. (The feel of this transition may be appreciated quite easily by stretching and bending an ordinary rubber band.) In turn, the slope of the volume vs. pressure function changes greatly between positive and negative transmural pressure scenarios with greatly increased compliance at negative transmural pressures. Further, the cross sectional shape of retinal veins, which was circular during expansion, becomes ovalized and ultimately flattened under negative transmural pressure. In this pressure range, as volume decreases during cardiac diastole, the observed longest diameter increases. The long diameters are perpendicular to the plane of observation during direct ophthalmoscopic examination, because the veins are compressed somewhat by the gel-like vitreous body against the underlying retina, choroid, and much stiffer sclera with a bias toward flattening between the vitreous body and the retina.

Visible pulsations in the long diameters of central veins close to the optic disc are large when transmural pressure cycles above and below a slightly negative mean value. This effect occurs because the largest changes in the major axis of a constant perimeter, ovalized elastic tube happen at volumes slightly less than the unstressed volume, $\hat{V}_0$, as shown in Appendix 2, Fig 14. For example, if the transmural pressure cycles through values consistently less than zero, as shown in Figures 8 and 11, modest changes in the long diameter, $\Delta d/\hat{d}_0$, will be seen with pulse inversion (increased diameter during emptying). If the transmural pressure cycles through values only slightly less than zero, relatively large changes in the long diameter, $\Delta d/\hat{d}_0$, will be seen.

The large size of observed changes in this regime depends on the dramatically reduced compliance of elastic tubes during bending, buckling, and flattening, compared to their compliance during circular expansion. However, if the transmural pressure cycles through only positive values, as shown in Figures 8 and 11, much smaller changes in $\Delta d/\hat{d}_0$ will be seen with a normal pulse shape (increased diameter during filling) owing to the greatly reduced compliance during wall stretching. The state change from expansion to buckling explains the presence of easily observed, retinal venous pulsations normally, and their apparent disappearance when the local internal venous pressure is elevated.

The pulsations happen in larger, downstream retinal veins close to the optic disc, because only in this region along their course is intravascular pressure less than intraocular pressure during all or part of the cardiac cycle under normal physiologic conditions. If local internal venous pressure is increased, for example, because of downstream compression of the central retinal vein in cases of intracranial hypertension, or because of local vasodilation; then transmural pressure in all of the retinal veins, including those close to the optic disc, may be positive throughout the entire cardiac cycle. In this regime of positive transmural pressure there is increased stiffness (reduced compliance) of the vascular wall. Pulsatile changes in observed diameter, $\Delta d/\hat{d}_0$, are greatly attenuated and may seem to disappear.

As Levin[1] noted "The reappearance of venous pulsations in three of seven unselected [normal] subjects on follow-up observation suggests that there is a precarious balance in some individuals between the various factors responsible for spontaneous venous pulsations." The present mathematical model elucidates the precarious balance of factors required for robust venous pulsations. These factors include mean arterial pressure, central venous pressure, intraocular pressure, and intracranial pressure, as well as local vascular compliance and resistance at various levels along the path of blood flow through the eye. An important part of the precarious balance relates to vasomotor tone in retinal arteries. If these arteries are normally constricted there will be sufficient pressure drop across them so that downstream retinal venous pressures close to the optic disc will be slightly less than intraocular pressure at some times during the cardiac cycle. Otherwise, the amplitude of retinal venous pulsations is greatly diminished.

Such complexity, however, need not be an excuse for inaction in the quest to harness improved understanding to achieve noninvasive estimation of intracranial pressure. Perhaps patient specific mathematical models could be implemented as smart phone applications to evaluate the critical intracranial pressure at which retinal venous pulsations seem to disappear. Inputs for the models might include arterial pressure measured with a standard cuff, intraocular pressure measured by tonometry or device such as a Diaton tonometer or Tonopen, central venous pressure measured by observation of the jugular veins at various degrees of head-of-bed elevation, and arteriolar resistance, estimated by observed diameters of retinal artery blood columns. Aggregation of such "soft" data could yield reasonable predictions that would be especially useful in patients in whom intracranial pressure could plausibly be rising, such as patients with intracranial tumors or patients with head trauma.

Conclusions

The present study is limited in that it is strictly theoretical in nature. Nevertheless, as a theoretical treatment, the proposed biomechanical model of retinal venous pulsations explains in a quantitative manner a number of heretofore unexplained or poorly explained phenomena:

- why spontaneous venous pulsations are usually confined to the most downstream retinal veins near the optic disc (lower internal pressure here compared with intraocular pressure)
- why spontaneous venous pulsations expand during cardiac diastole (ovalization and the long diameter vs. volume curve)
- why spontaneous venous pulsations are sometimes absent in normal individuals (relatively low intraocular pressure or high cavernous sinus pressure)
- why increased intracranial pressure can cause spontaneous venous pulsation to seemingly vanish (nonlinear compliance)
- why digital pressure on the globe can restore spontaneous venous pulsations (transmural pressure balance)
- why spontaneous venous pulsations can appear in glaucoma (raised intraocular pressure)
- why retinal arterial pulsations are normally nil or minimal (consistently positive transmural pressure in a low compliance domain)
- why collapse of the central retinal vein is not observed during its intraneural course in the optic nerve stem (Fry[12], thick walled cylinder equations – Appendix 1)

The ultimate validity and usefulness of these theoretical ideas awaits follow-on clinical testing and application.

Acknowledgments

None.

References

1. Levin BE (1978) The clinical significance of spontaneous pulsations of the retinal vein. Arch Neurol 35: 37-40.
2. Morgan WH, Lind CR, Kain S, Fatehee N, Bala A, et al. (2012) Retinal vein pulsation is in phase with intracranial pressure and not intraocular pressure. Invest Ophthalmol Vis Sci 53: 4676-4681.
3. Kim M, Lee EJ, Seo JH, Kim TW (2014) Relationship of spontaneous retinal vein pulsation with ocular circulatory cycle. PLoS One 9: e97943.
4. Wong SH, White RP (2013) The clinical validity of the spontaneous retinal venous pulsation. J Neuroophthalmol 33: 17-20.
5. Jacks AS, Miller NR (2003) Spontaneous retinal venous pulsation: aetiology and significance. J Neurol Neurosurg Psychiatry 74: 7-9.
6. Kahn EA, Cherry GR (1950) The clinical importance of spontaneous retinal venous pulsation. Med Bull (Ann Arbor) 16: 305-308.
7. Walsh TJ, Garden JW, Gallagher B (1969) Obliteration of retinal venous pulsations during elevation of cerebrospinal-fluid pressure. Am J Ophthalmol 67: 954-956.
8. LoZito JC (1977) Retinal spontaneous venous pulsations in neurologically ill patients: incidence and significance. J Fla Med Assoc 64: 355-357.
9. Ropper A, Samuels M, Klein J (2014) Adams and Victor's Principles of Neurology. New York: McGraw-Hill Medical.
10. Miller N, Newman N, Biousse V, Kerrison J (2005) Walsh & Hoyt's Clinical Neuro-Opthalmology, 6th Edition. Philadelphia: Williams & Wilkins.
11. Hayreh SS (1963) The Central Artery of the Retina. Its Role in the Blood Supply of the Optic Nerve. Br J Ophthalmol 47: 651-663.
12. Fry W (1931) The Pathology of Papilledema: An examination of forty eyes with special reference to compression of the central vein of the retina. American Journal of Ophthalmology 14: 874-883.
13. Geddes LA, Baker LE (1975) Prinicples of Applied Biomedical Instrumentation, Second edition.
14. Bergel DH (1961) The static elastic properties of the arterial wall. J Physiol 156: 445-457.
15. Moreno AH, Katz AI, Gold LD, Reddy RV (1970) Mechanics of distension of dog veins and other very thin-walled tubular structures. Circ Res 27: 1069-1080.
16. Lagreze WA, Gaggl M, Weigel M, Schulte-Monting J, Buhler A, et al. (2009) Retrobulbar optic nerve diameter measured by high-speed magnetic resonance imaging as a biomarker for axonal loss in glaucomatous optic atrophy. Invest Ophthalmol Vis Sci 50: 4223-4228.
17. Lee SB, Uhm KB, Hong C (1998) Retinal vessel diameter in normal and primary open-angle glaucoma. Korean J Ophthalmol 12: 51-59.
18. Boron WF, Boulpaep EL (2005) Medical Physiology. Philadelphia: Elsevier. 1319 p.
19. Permutt S, Riley RL (1963) Hemodynamics of Collapsible Vessels with Tone: The Vascular Waterfall. J Appl Physiol 18: 924-932.
20. Avery RA, Shah SS, Licht DJ, Seiden JA, Huh JW, et al. (2010) Reference range for cerebrospinal fluid opening pressure in children. N Engl J Med 363: 891-893.
21. Heil M, Pedley TJ (1996) Large post-buckling deformations of cylindrical shells conveying viscous flow. Journal of Fluids and Structures 10: 565-599.
22. Karamanos S (2002) Bending instabilities of elastic tubes. International Journal of Solids and Structures 39: 2059-2085.
23. Kresch E, Noordergraaf A (1972) Cross-sectional shape of collapsible tubes. Biophys J 12: 274-294.
24. Kresch E (1977) Cross-sectional shape of flexible tubes. Bull Math Biol 39: 679-691.
25. Levine DN (1998) Spontaneous pulsation of the retinal veins. Microvasc Res 56: 154-165.

26. Bellezza AJ, Hart RT, Burgoyne CF (2000) The optic nerve head as a biomechanical structure: initial finite element modeling. Invest Ophthalmol Vis Sci 41: 2991-3000.
27. Ruiz-Teran A, Gardner L (2008) Elastic buckling of elliptical tubes. Thin-Walled Structures 46: 1304-1318.
28. Chow KW, Mak CC (2006) A simple model for the two dimensional blood flow in the collapse of veins. J Math Biol 52: 733-744.

Appendix 1: biomechanics of the central retinal vein within the optic nerve stem

To determine the degree of compression of the central retinal vein within the optic nerve stem, one may regard the vein, surrounded by nerve tissue, as a thick walled pressure vessel. The outer wall of the pressure vessel is the outer surface of the optic nerve, surrounded by the subarachnoid space. The inner wall of the pressure vessel is the outer wall of the intraneural portion of the central retinal vein. Forces from circumferential stretching of the nerve add to forces from circumferential stretching of the wall of the vein.

Stresses and strains within the walls of thick walled pressure vessels of cylindrical geometry are described by the Lame equations. Let ε denote strain and σ denote stress. Let subscript, θ, indicate the circumferential or hoop dimension. Hoop strain ε_θ is the change in circumference divided by the reference circumference. Because of cylindrical geometry, the hoop strain is the same as the fractional change in radius at any particular radius, r. Thus for a thick walled cylindrical pressure vessel the fractional expansion or compression of the in the hoop dimension at radius, r, equals the fractional expansion or compression of the diameter of the vessel at radius, r. In this analysis the relevant Lame equation is

$$\varepsilon_\theta = \frac{1}{E_{nerve}}\left(\sigma_\theta - \sigma_r\right), \tag{13}$$

where ε_θ is hoop strain, E_{nerve} is Young's modulus of elasticity of nerve tissue, σ_θ is hoop stress, and σ_r is radial stress. The Lame equations for hoop and radial stress as a function of external pressure, P_o, internal pressure, P_i, and variable radial distance, r, within the wall of the pressure vessel are

$$\sigma_\theta = \frac{r_i^2 P_i - r_o^2 P_o}{r_o^2 - r_i^2} + \frac{\left(P_i - P_o\right) r_i^2 r_o^2}{\left(r_o^2 - r_i^2\right) r^2} \tag{14}$$

$$\sigma_r = \frac{r_i^2 P_i - r_o^2 P_o}{r_o^2 - r_i^2} - \frac{\left(P_i - P_o\right) r_i^2 r_o^2}{\left(r_o^2 - r_i^2\right) r^2}. \tag{15}$$

Noting that the first terms in the above expressions are the same and that the second terms are opposite in sign, we have for $r = r_i$, at the outer wall of the central retinal vein,

$$\varepsilon_\theta = \frac{2}{E_{nerve}}\left(\frac{(P_i - P_o)r_o^2}{(r_o^2 - r_i^2)}\right). \quad (16)$$

This is the fractional change in inner radius of the nerve adjacent to the outer wall of the central retinal vein. Further, for $r_i << r_o$ in the present case (the central retinal vein being much smaller in diameter than the optic nerve)

$$\varepsilon_\theta \approx \frac{2}{E_{nerve}}(P_i - P_o), \quad (17)$$

and the change in strain for a given change in cerebrospinal fluid pressure, is

$$\Delta\varepsilon_\theta \approx \frac{2}{E_{nerve}}\Delta(P_i - P_o) = -\frac{2\Delta P_o}{E_{nerve}}. \quad (18)$$

Assuming a Young's modulus of nerve tissue[26] of 55 kPa = 550 x 10^3 dynes/cm^2. We have for a large pathological change in cerebrospinal fluid pressure of 20 mmHg.

$$\Delta\varepsilon_\theta \approx -\frac{2\cdot 20\cdot 1333\,\text{dynes/cm}^2}{550\cdot 10^3\,\text{dynes/cm}^2} = -0.1.$$

This is a maximal 10 percent decrease in the radius of the central retinal vein caused by pathologically high cerebrospinal pressure. Thus, he optic nerve largely protects the intraneural portion of the central retinal vein from collapsing. Further, because of the thick protective wall of the surrounding nerve, it is reasonable to assume that there will be circular deformation in both expansion and compression. The optic nerve acts as a splint to prevent the vein from ovalizing and flattening during its intraneural course. In this case the local compliance remains linear, even with internal pressure less than external pressure.

To specify the compliance of the nerve tissue surrounding the central retinal vein in the form of a thick walled cylinder, note that

$$\Delta\varepsilon_\theta \approx \frac{2}{E_{nerve}}\Delta(P_i - P_o) = \frac{2}{E_{nerve}}\Delta P. \quad (19)$$

Introducing the volume, V, of blood in the vein, having radius r_0 at the reference pressure, and considering small changes in radius, Δr,

$$\frac{\Delta V}{V_0} = \frac{\pi(r_0 + \Delta r)^2 - \pi r_0^2}{\pi r_0^2} = \frac{r_0^2 + 2r_0\Delta r + (\Delta r)^2 - r_0^2}{r_0^2} \approx 2\frac{\Delta r}{r_0} = 2\Delta\varepsilon_\theta = \frac{4}{E_{nerve}}\Delta P. \quad (20)$$

The compliance of the thick walled pressure vessel is thus

$$C_{thick} = \frac{\Delta V}{\Delta P} \approx \frac{4}{E_{nerve}} V_0 . \tag{21}$$

If C_{thin} is the compliance of the vein itself as a thin walled pressure vessel with Young's modulus E_{wall}, given by body text Equation (1), namely $C = \frac{2\pi L r_i^3}{E_{wall} h}$, then the total pressure change, ΔP, in the vein surrounded by nerve for a given volume change, ΔV, is

$$\Delta P = \Delta V \left(\frac{1}{C_{thin}} + \frac{1}{C_{thick}} \right) = \frac{\Delta V}{C_{thin}} \left(1 + \frac{C_{thin}}{C_{thick}} \right). \tag{22}$$

The ratio C_{thin} / C_{thick} is given by

$$\frac{C_{thin}}{C_{thick}} = \frac{\frac{2V_0}{E_{wall}} \cdot \frac{r_0}{h_0}}{\frac{4V_0}{E_{nerve}}} = \frac{1}{2} \frac{E_{nerve}}{E_{wall}} \frac{r_0}{h_0} . \tag{23}$$

Taking the ratio of E_{nerve}/E_{wall} to be approximately 1/100 (55 kPa/5,000 kPa, see[26] and[14]) and $r_0/h_0 = 10$ for the retinal vein[16], we have

$$\Delta P \approx \frac{\Delta V}{C_{thin}} (1.1). \tag{24}$$

The compliance of the vein plus nerve system is quite similar to the compliance of the vein alone. The major difference is that the surrounding nerve inhibits flattening of the vein under negative transmural pressure. Ovalization and flatting happen instead in the region where the central retinal vein travels through the subarachnoid space.

Appendix 2: long diameter vs. volume function for a partially flattened tube of constant perimeter (racetrack model)

The exact solution for the shape of a partially flattened elastic tube is highly complex and empirical in nature[15,23,27]. However, based on the studies of Chow and Mak[28], the complex geometry can be approximated by a series of well defined geometric figures, including racetrack shaped, dog bone shaped, and flat models. Numerical comparisons of the models (data not shown) suggest that over the entire range of empirical cross sections, the racetrack model has the best overall performance with correct limiting values and realistic intermediate values.

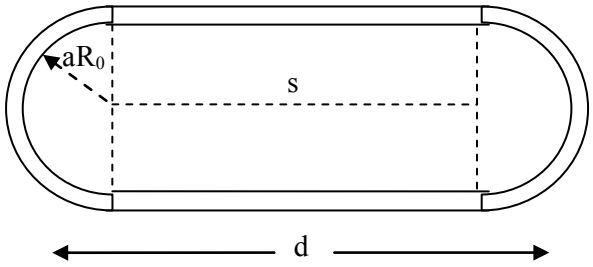

Fig 13. Sketch of an analytical model for fluid flow in a tube having a racetrack shaped cross section.

Fig 13 shows a racetrack shaped cross section of a collapsible tube. The flat middle section has length, s, and the semicircular ends have radii, aR_0, where $0 \le a \le 1$ is a flattening parameter, a = 1 indicating no flattening, and a = 0 indicating complete flattening. The long internal diameter of the cross section (corresponding to opthalmoscopically visible blood in a retinal vein) is denoted d. The short internal diameter of the cross section is $2aR_0$. The perimeter of the inside of the tube is $2\pi aR_0 + 2s$. During flattening one can assume that the perimeter remains constant at the unstressed value, $2\pi R_0 = 2\pi aR_0 + 2s$. Solving the forgoing expression for straight length, s, with the constant perimeter constraint, gives $s = \pi R_0(1 - a)$. Thus, when a = 1, s = 0, and when a = 0, $s = \pi R_0$. The perimeter of the completely flattened structure is $2\pi R_0$, as expected.

The long diameter of the racetrack shaped cross section is $d = 2aR_0 + s = 2aR_0 + \pi R_0(1 - a)$. The original long diameter of the unstressed tube is $2R_0$. Hence, the ratio

$$\frac{d}{\hat{d}_0} = a + \frac{\pi}{2}(1-a)\,. \qquad (25)$$

When a = 1, indicating no flattening, $d/\hat{d}_o = 1$. When a = 0, indicating complete flattening, $d/\hat{d}_o = \pi/2 \approx 1.57$. To express the flattening factor, a, in terms of the relative volume or area, compared to unstressed volume or area we have $\text{Area} = \pi a^2 R_0^2 + (2aR_0)s$. For the constant perimeter constraint $s = \pi R_0(1-a)$, so

$$\text{Area} = \pi a^2 R_0^2 + (2aR_0)\pi R_0(1-a) = \pi R_0^2\left(a^2 + 2a(1-a)\right) = \pi R_0^2\left(2a - a^2\right).$$

The ratio of flattened area or volume to un-flattened area or volume is thus $V/V_0 = 2a - a^2$. Solving this quadratic equation for flattening factor, a, in terms of the volume ratio, V/V_0, gives $a = 1 - \sqrt{1 - V/V_0}$. Hence, for the racetrack approximation the diameter vs. volume relationship during flattening is

$$\frac{d}{d_0} = a + \frac{\pi}{2}(1-a) = 1 - \sqrt{1 - V/V_0} + \frac{\pi}{2}\sqrt{1 - V/V_0} \qquad (26)$$

or

$$\frac{d}{d_0} = 1 + \left(\frac{\pi}{2} - 1\right)\sqrt{1 - V/V_0} \approx 1 + 0.57\sqrt{1 - V/V_0}\,. \qquad (27)$$

A plot of this relationship, and for expanding deformation, $d/d_0 = \sqrt{V/V_0}$, is shown in Fig 14.

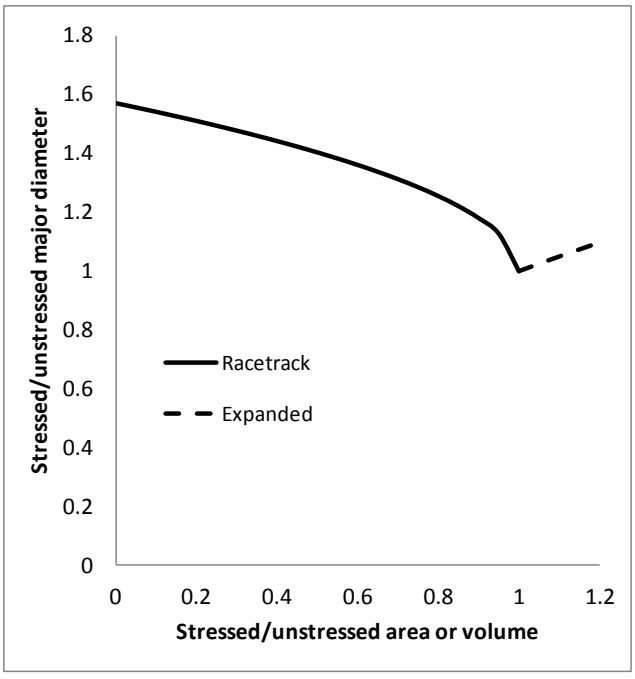

Fig 14. Changes in major diameter as a function of volume for model retinal veins.

Appendix 3: resistance to axial blood flow in constant perimeter, ovalized vessels (racetrack model)

Blood flow in a tube can be modeled as movement of concentric, sleeve-like shells or laminae of fluid as shown in Fig 15. Consider a slug of fluid of length, L, having axial pressure difference, ΔP, across it and a racetrack shaped cross section. We need to compute volumetric flow for a racetrack shape, approximating a partially collapsed, elastic tube, as shown in Fig 13 in Appendix 2. A center section of length, s, is flattened. The ends are semi-circular in shape with maximal inner radius, R. In the axial dimension there is laminar flow. Thin shells of fluid at variable distance, r, from the centerline also have racetrack shapes having straight segments of length, s, and curved ends of radius, r. For a family of racetracks of constant perimeter, considered later, the parameters R and s will vary, depending on the degree of flattening. For now, however, length, s, is a constant for any given racetrack.

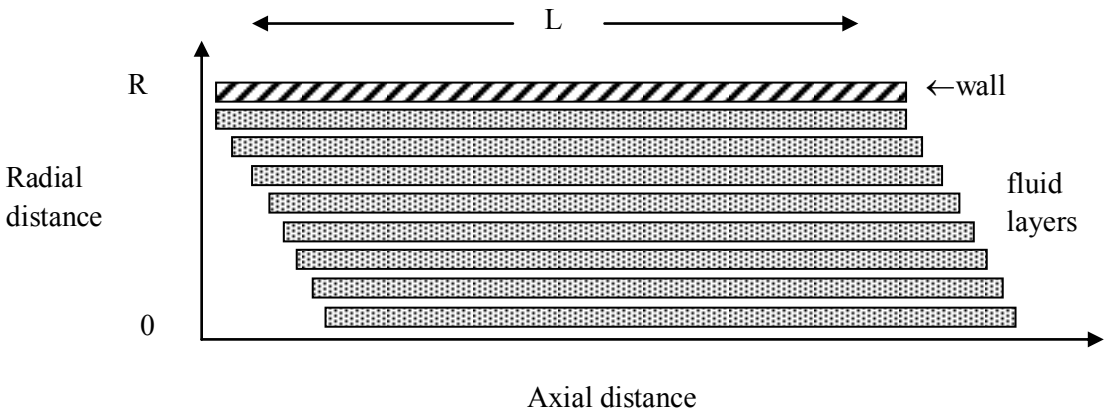

Fig 15. Laminar flow in the axial dimension of a partially flattened tube.

For a classical Newtonian fluid the viscous force between layers of shared surface area, A, separated by distance Δr is

$$F = \mu A \frac{\Delta u}{\Delta r}, \tag{28}$$

where μ is the viscosity, and $u(r)$ is the velocity of the shell at distance, r. For a fluid shell moving at constant velocity, u, at distance, r, Newton's second law (force = mass x acceleration) with fluid density, ρ, is

$$F = \Delta P \cdot (2\pi r + 2s) \cdot \Delta r + F_\mu = \rho \cdot (2\pi r + 2s) L \Delta r \frac{du}{dt} = 0, \tag{29}$$

where, F_μ, is the net viscous force acting on both sides of the shell at radius, r. For quasi-steady flow ($du/dt \approx 0$) we have under the steady flow assumption

$$\Delta P \cdot \Delta r + \frac{F_\mu}{2\pi(r + s/\pi)} = 0. \tag{30}$$

As shown in Box 1, the net viscous force,

$$F_\mu = 2\pi(r + s/\pi)\mu L \left(\frac{d^2u}{dr^2} + \frac{1}{r + s/\pi} \frac{du}{dr} \right) \Delta r, \tag{31}$$

so that the expanded version of Expression (30) becomes

$$0 = \Delta P \cdot \Delta r + \mu L \left(\frac{d^2u}{dr^2} + \frac{1}{r + s/\pi} \frac{du}{dr} \right) \Delta r,$$

or

$$\frac{d^2u}{dr^2} + \frac{1}{r + s/\pi} \cdot \frac{du}{dr} + \frac{\Delta P}{\mu L} = 0. \tag{32}$$

This is the fundamental differential equation for fluid velocity during steady laminar flow.

Box 1: viscous forces on a racetrack shaped shell of fluid in a tube

From the definition of viscosity, $F = \mu A \frac{\Delta u}{\Delta r}$, the viscous forces acting on both the outside surface and the inside surfaces of a shell of fluid that is Δr thick at radius, r, are given by

$$\begin{aligned} F_\mu &= \frac{\mu L}{\Delta r}\left\{2\pi\left(r+\frac{s}{\pi}+\frac{\Delta r}{2}\right)\big(u(r+\Delta r)-u(r)\big)+2\pi\left(r+\frac{s}{\pi}-\frac{\Delta r}{2}\right)\big(u(r-\Delta r)-u(r)\big)\right\} \\ &= \frac{2\pi(r+s/\pi)\mu L}{\Delta r}\left\{\left(1+\frac{1}{2}\frac{\Delta r}{r+s/\pi}\right)\big(u(r+\Delta r)-u(r)\big)+\left(1-\frac{1}{2}\frac{\Delta r}{r+s/\pi}\right)\big(u(r-\Delta r)-u(r)\big)\right\} \\ &= \frac{2\pi(r+s/\pi)\mu L}{\Delta r}\left\{\begin{array}{l} u(r+\Delta r)+u(r-\Delta r)-2u(r) \\ +\frac{1}{2}\frac{\Delta r}{r+s/\pi}\big(u(r+\Delta r)-u(r)-u(r-\Delta r)+u(r)\big)\end{array}\right\}. \end{aligned}$$

Passing to the derivative,

$$F_\mu = \frac{2\pi(r+s/\pi)\mu L}{\Delta r}\left\{\left(\frac{d^2u}{dr^2}\right)(\Delta r)^2+\frac{1}{2}\frac{\Delta r}{r+s/\pi}\left(\frac{du}{dr}\right)\cdot 2\Delta r\right\}, \text{ or}$$

$$F_\mu = 2\pi(r+s/\pi)\mu L\left(\frac{d^2u}{dr^2}+\frac{1}{r+s/\pi}\frac{du}{dr}\right)\Delta r.$$

Solution of Equation (32): Consider a possible solution of the general form

$$u = a\left(k-\frac{s}{\pi}r-\frac{1}{2}r^2\right) \qquad (33a)$$

$$\frac{du}{dr} = -a\left(r+\frac{s}{\pi}\right) \qquad (33b)$$

$$\frac{d^2u}{dr^2} = -a \qquad (33c)$$

where a and k are constants to be determined.

Now using the method of undetermined coefficients to solve for constants, a and k, we have by back substitution into Equation (32), namely, $\frac{d^2u}{dr^2}+\frac{1}{r+s/\pi}\cdot\frac{du}{dr}+\frac{\Delta P}{\mu L}=0$,

$$-a+\frac{1}{r+s/\pi}\cdot -a\left(r+\frac{s}{\pi}\right)+\frac{\Delta P}{\mu L}=0\text{, or } -2a+\frac{\Delta P}{\mu L}=0\text{, giving} \tag{34a}$$

$$a=\frac{\Delta P}{2\mu L} \tag{34b}$$

Invoking the boundary condition that when r = R, u = 0 in Equation (33a) gives

$$k=R\left(\frac{s}{\pi}+\frac{1}{2}R^2\right), \tag{35}$$

and combining (33a), (34b), and (35) gives the velocity profile as a function of distance, r, namely

$$u(r)=\frac{\Delta P}{2\mu L}\left(R\left(\frac{s}{\pi}+\frac{1}{2}R^2\right)-\frac{s}{\pi}r-\frac{1}{2}r^2\right), \text{ or}$$

$$u(r)=\frac{\Delta P}{4\mu L}\left(R^2-r^2+2\frac{s}{\pi}(R-r)\right). \tag{36}$$

When r = 0, the centerline flow velocity is maximal. When r = R, the boundary condition, flow velocity is zero.

Total volumetric flow, Q, in units such as ml/sec, and in turn the resistance of the racetrack shaped tube are obtained by integration.

$$dQ=(2\pi r+2s)\cdot dr\cdot u(r)=(2\pi r+2s)\frac{\Delta P}{4\mu L}\left(R^2-r^2+2\frac{s}{\pi}(R-r)\right)dr \text{ , and } Q=\int_0^R dQ\,.$$

After multiplication and integration one obtains,

$$Q=\frac{\pi\Delta P R^4}{8\mu L}\left[1+\frac{4}{\pi}\frac{s}{R}+\frac{4}{\pi^2}\frac{s^2}{R^2}\right]. \tag{37}$$

If s = 0 Equation (37) is Poiseuille's law for laminar flow in a cylindrical tube.

The resistance to flow in the tube is the ratio of pressure difference between the ends divided by flow. Here the resistance is

$$\tilde{R} = \frac{\Delta P}{Q} = \frac{8\mu L}{\pi R^4} \cdot \frac{1}{1 + \frac{4}{\pi}\frac{s}{R} + \frac{4}{\pi^2}\frac{s^2}{R^2}} \tag{38}$$

Equation (38) describes resistance in a generalized tube with parameters R and s having a racetrack shaped cross section, not a constant perimeter tube. Next we introduce the constant perimeter constraint for an elastic tube with initial circular radius R_0 in the unstressed state that subsequently undergoes flattening into a quasi-racetrack configuration with constant perimeter. The constant perimeter constraint is $2\pi R_0 = 2\pi R + 2s$ or $s = \pi(R_0 - R)$. If the flattened end-radius $R = aR_0$, for flattening factor, a, then

$$s = \pi R_0 (1 - a). \tag{39}$$

Substituting in Equation (38) and simplifying yields an expression for the resistance, $\tilde{R}$, to fluid flow in an elastic tube having a racetrack shaped cross section and constant perimeter.

$$\tilde{R} = \frac{\Delta P}{Q} = \frac{8\mu L}{\pi R_0^4} \cdot \frac{1}{a^4 + 4a^2(1-a)}. \tag{40}$$

To express the flattening factor, a, in terms of the relative volume or area, compared to unstressed volume or area, we have $\text{Area} = \pi a^2 R_0^2 + (2aR_0)s$. For the constant perimeter constraint $s = \pi R_0 (1 - a)$, and in turn

$$\text{Area} = \pi a^2 R_0^2 + (2aR_0)\pi R_0(1-a) = \pi R_0^2\left(a^2 + 2a(1-a)\right) = \pi R_0^2\left(2a - a^2\right). \tag{41}$$

The ratio of flattened area or volume to un-flattened area or volume is thus $V/V_0 = 2a - a^2$. Solving this quadratic equation for flattening factor, a, in terms of the volume ratio, V/V_0, gives $a = 1 - \sqrt{1 - V/V_0}$, which can be used in Equation (40) to compute resistance to blood flow in the partially flattened tube.